Catalysis Today 160 (2011) 109–115

Contents lists available at ScienceDirect

Catalysis Today

journal homepage: www.elsevier.com/locate/cattod

PtRuP nanoparticles supported on mesoporous carbon thin film as highly active anode materials for direct methanol fuel cell☆

Meng-Liang Lin[a], Man-Yin Lo[b], Chung-Yuan Mou[a,*]

[a] Department of Chemistry and Center of Condensed Matter Science, National Taiwan University, 1 Roosevelt Rd., Sec. 4, Taipei 106, Taiwan
[b] Material and Chemical Research Laboratories, Industrial Technology Research Institute, Hsinchu 300, Taiwan

ARTICLE INFO

Article history:
Available online 15 June 2010

Keywords:
Mesoporous carbon
PtRu alloy
Direct methanol fuel cell
Phosphorus
EXAFS
Size effect

ABSTRACT

PtRu nanocatalyst supported on mesoporous carbon thin film (TFC) with incorporation of the non-metallic phosphorus is explored as an anodic catalytic material for direct methanol fuel cell (DMFC). The catalyst 20 wt.% $PtRuP_{0.1}$/TFC gives a very high current density in the electrochemical oxidation of methanol, which is much enhanced than that of the PtRu/TFC without P loading and two times higher compared to a commercial PtRu/XC-72 catalyst. XPS and EXAFS analysis of the catalysts show that phosphorus helps to reduce the size of PtRu nanoalloy by acting as a surface protecting agent to the nanoparticles and it does not alter the electronic structure of PtRu. The PtRuP nanocatalyst with a particle size of 3 nm was found to have the best reactivity and catalytic stability.

1. Introduction

Anodic catalytic material for direct methanol fuel cell (DMFC) has been receiving increasing attention in its detailed nanostructure [1–3]. One needs to have precise manipulation in structure and composition of the electrocatalyst in order to achieve substantial improvement in its performance. In most of the new developments, one mainly worked on Pt-based nanoparticles supported on conductive porous carbon which is in turn deposited on the electrode. There are many factors affecting the performance of the anode: (1) pore structure of the carbon materials to facilitate good transport of electrons and fuel molecules, (2) the second and other elements in alloying with Pt to avoid CO poisoning, (3) the size of the metal nanoparticle, and (4) the surface composition of the Pt-based alloy nanoparticles. It is necessary to combine and optimize all the above factors to achieve good performance of the anodic material for DMFC.

For the carbon support materials in anode, ordered mesoporous carbon (OMC) has the advantages of high surface area, tunable pore size, interconnected pore network, and tailorable surface properties [4]. Various designing features for electrode materials have been emphasized in recent reports [5–8]. Recently, we have presented a novel OMC of CMK-3 type thin film of high surface area to increase dispersion of metal nanocatalysts and with very short perpendicular (to electrode) nanochannels to facilitate the transport of reactants and products [9]. The thin film morphology simultaneously improved its electric contact with electrode surface and the mass transport of the reactants in and out of the short channels where metal nanoparticles are confined.

The Pt-based bimetallic catalyst (often with Ru) is considered the best strategy to give catalytic synergy in enhancing both reactivity and stability for electrooxidation of methanol. However, the bifunctionality can be lost from the electrochemical dissolution of the less noble component of the alloy [10]. For long-term operation of the anodic material in acidic medium of DMFC, the second metal is gradually lost and accompanied by extensive aggregation and CO poisoning on Pt. This decreases the efficiency of catalytic current density of the nanosized particles. Liang et al. studied the stabilization of PtRu by gold and found that the dissolution of Ru can be reduced substantially [11]. Wang et al. incorporated nickel in the PtRu bimetallic nanoparticle and obtained much enhanced catalytic performance and CO tolerance [12]. The third incorporated transition metal elements include RhNi [13], Ir [14] and Co [15,16]. Their effects are most probably in altering the electronic structure of Pt-based nanoparticle in effecting catalytic synergy.

The other approach to have PtRu alloy with high activity and well-preserved bifunctionality is to decrease the size of the bimetallic PtRu nanoparticle [17–19]. For example, nanosized PtRu particles were synthesized by colloid method using ethylene glycol as the stabilizer [20,21]. However, before carrying out the catalysis reaction, the stabilizer needs to be removed and it often leads to sintering in the process. In another approach, the addition of a non-metallic element, such as N, S or P, for the dispersion

☆ This paper is for a special issue entitled "Heterogeneous Catalysis by Metals: New Synthetic Methods and Characterization Techniques for High Reactivity" guest edited by Jinlong Gong and Robert Rioux.

* Corresponding author. Tel.: +886 2 3366 5251; fax: +886 2 2366 0954.
E-mail address: cymou@ntu.edu.tw (C.-Y. Mou).

0920-5861/$ – see front matter © 2010 Elsevier B.V. All rights reserved.
doi:10.1016/j.cattod.2010.05.018

of Pt-based nanoparticle has been found to be effective [22–25]. The element phosphorus is found to reduce the size of Pt particle notably better by generating Pt–P and Ru–P interactions in a stable way [22]. It has been shown that the growth of PtRu is suppressed by the incorporation of P. However, the perturbation on the electronic structure of PtRu by phosphorus is not clear. Detailed microscopic understanding of the effect of P on the catalytic nanoparticle is still lacking. Herein, we report a PtRu nanocatalyst supported on mesoporous carbon thin film with the incorporation of phosphorus. The catalyst system gave superior electrocatalytic activity compared to the one without P loading. With detailed EXAFS and XPS analysis, we can understand the electronic structure and composition of the P-modified bimetallic PtRu nanoparticle. The best bifunctional synergy and catalytic stability for the electrooxidation of methanol is found with a PtRuP alloy size of 3 nm. Together with the special nanostructure of the carbon thin film support of perpendicular nanochannel, the PtRuP/meso-C catalyst system is found to give very high electrocatalytic activity for DMFC.

2. Experimental

2.1. Preparation of TFC carbon and supported PtRuP catalyst

In the first step, ordered mesoporous carbon thin film with perpendicular channels (TFC) was synthesized according to our previously reported method [9]. Repeated loading of sucrose, dehydration by concentrated sulfuric acid, and complete carbonization at 900 °C were performed. The silica content was then dissolved with 10 wt.% hydrogen fluoride solution to recover the TFC carbon product.

The bimetallic PtRu with the non-metallic additive of phosphorus was synthesized and deposited on carbon support using a wet-chemical reduction method. 0.1 g of TFC material was added to a solution containing desired amount of 0.01 M H_2PtCl_6 (Acrôs), 0.01 M $RuCl_3$ (Aldrich), and 0.01 M NaH_2PO_2 (Acrôs). The mixture was stirred for 0.5 h, and an excess of 0.1 M $NaBH_{4(aq)}$ solution was added into the mixture drop by drop. After stirring for another hour, the solid suspension was recovered by centrifugation, washing with water twice, and drying in air at 60 °C. The product was denoted as PtRu/TFC or $PtRuP_X$/TFC (with nominal P content of $X = 0.05$, 0.1, and 0.2).

2.2. Electrochemical activity tests

The electrochemical activity measurements were carried out by cyclic voltammetry (CV) using an Autolab PGSTAT 30 potentiostat equipped with a rotatory disk electrode (RDE) [26]. A conventional three-compartment electrochemical cell consisting of glassy carbon (GC) electrode with an area of 0.196 cm^2 as the working electrode, Pt as the counter electrode, and reference hydrogen electrode (RHE) as the reference electrode was used. The GC electrode was polished to a mirror finish with a 0.05 μm alumina suspension before each experiment. The catalyst ink was prepared by adding 5 mg of the catalyst in 2.5 ml water and ultrasonically dispersed for 0.5 h. Then, 20 μL of suspension was pipetted onto the top surface of a GC electrode, followed by drying at 60 °C for 1 h in air. A metal loading at 0.04 mg/cm^2 on the working electrode was obtained. After the electrode was cooled down to room temperature, 20 μL of 1 wt.% Nafion® solution was pipetted onto the ink surface. CV study of methanol oxidation was measured in 0.5 M H_2SO_4 and 1.0 M CH_3OH solution at 60 °C with a scan rate of 10 mV/s and working electrode rotating at 1600 rpm. The electrochemical activity was characterized by the steady-state current density at 0.5 V.

2.3. Structure and elemental characterization

The powder XRD patterns were collected on a PANalytical X'Pert PRO instrument operating at 45 kV and 40 mA with Cu Kα ($\lambda = 1.5406$ Å) radiation. Nitrogen adsorption characterizations were conducted at −196 °C on a Micromeritics ASAP 2010 apparatus. The specific surface area of the sample was calculated according to the Brunauer–Emmett–Teller (BET) method, and the Barrett–Joyner–Halenda (BJH) method for estimating pore size distribution. TEM images were obtained using a Hitachi H-7100 instrument with an operating voltage of 75 kV SEM images were taken with a JSM-6700F microscope (JEOL) operating at 10 kV. Elemental analysis was determined by inductively coupled plasma atomic emission spectroscopy (ICP-AES) using a Jarrel-Ash ICAP 9000 instrument. XPS measurements were performed with a Thermo VG Scientific, ESCALAB 250 equipped with an Al Kα radiation source (1486.6 eV) under a residual pressure of $\sim 1 \times 10^{-9}$ Torr. For analysis, the spectra were deconvoluted by a least-squares procedure to a product of Gaussian–Lorentzian functions after background subtraction using XPSPEAK software.

X-ray absorption spectra (XAS) were recorded at beamline 01C1 of the National Synchrotron Radiation Research Center (NSRRC) of Taiwan. The electron storage ring is operated at 1.5 GeV and 300 mA. A double Si(1 1 1) crystal monochromator was employed for energy selection with a resolution $\Delta E/E$ better than 1×10^{-4} at Pt L_{III}-edge and Ru K-edge. All the experiments were conducted in a stainless steel cell with Krypton film cap in two sides for beam path to avoid exposure of air. Before each measurement, the sample was reduced with 10% H_2 for 0.5 h to remove the surface oxygen. All spectra were recorded at room temperature in a transmission mode, and with the double-crystal monochromator detuned to eliminate the effect of higher harmonics in the X-ray beam. A standard compound (Pt foil or Ru powder) was measured simultaneously so that energy calibration could be performed scan by scan. Raw XAS data were analyzed following standard procedures.

The EXAFS function was obtained by subtracting the post-edge background from the overall absorption and normalized with respect to the edge jump step. The normalized $\chi(E)$ was transformed from energy space to k-space with $\chi(k)$ multiplied by k^3 to compensate for EXAFS oscillations in the high-k region. Subsequently, k^3-weighted $\chi(k)$ data in k-space ranging from 3.0 to 14.3 $Å^{-1}$ for the Pt L_{III}-edge and from 3.5 to 12.9 $Å^{-1}$ for the Ru K-edge were Fourier transformed to r-space. A nonlinear least-squares curve fitting was carried out with regard to the data in r-space ranging from 1.60 to 3.10 Å for Pt and from 1.69 to 3.10 Å for Ru. Reference phase and amplitude for the Pt–Pt and Ru–Ru coordination shells were each obtained from a Pt foil and a Ru powder. All the computations were implemented in the UWXAFS software package with the backscattering amplitude and phase shift for the atom pairs being calculated using FEFF 7 code [27].

3. Results and discussion

3.1. Synthesis and characterization of carbon-supported nanocatalysts

By impregnating carbon supports with platinum, ruthenium, and phosphorus sources and reducing chemically with sodium borohydride, PtRuP nanoparticles are homogeneously dispersed onto the external and internal surfaces of mesoporous carbon thin film. Fig. 1 shows the XRD patterns of 20 wt.% PtRuP/TFCs with different nominal ratios of phosphorus. All of the samples give similar diffraction profiles of face-centered cubic (fcc) structure of Pt crystallites, with the (2 2 0) diffraction peaks shifting from about 67.5° to 68.0°, corresponding to a decrease in the lattice constant due

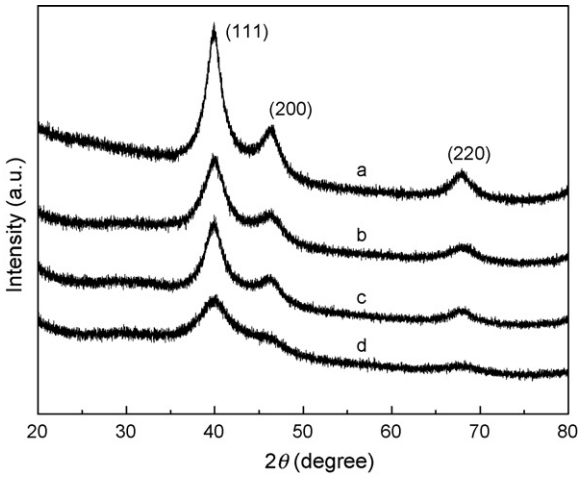

Fig. 1. Wide-angle XRD patterns of (a) PtRu/TFC, (b) $PtRuP_{0.05}$, (c) $PtRuP_{0.1}$, and (d) $PtRuP_{0.2}$ samples with total 20 wt.% metal loadings.

Table 1
Nitrogen adsorption–desorption characteristics of selected samples.

Sample	BET surface area (m^2/g)	Pore volume[a] (cm^3/g)	BJH pore size (nm)
PtRu/TFC	926	0.96	4.0
$PtRuP_{0.05}$/TFC	746	0.68	4.0
$PtRuP_{0.1}$/TFC	773	0.66	4.0
$PtRuP_{0.2}$/TFC	768	0.64	4.0

[a] Total pore volume is obtained from $p/p_0 = 0.99$.

to the incorporation of Ru atoms [28]. No recognizable Ru hexagonal close-packed (hcp) structure or RuO_2 tetragonal phase was observed in all of the samples, suggesting that Ru was mostly incorporated into Pt fcc lattice and formed Pt–Ru bimetallic alloy [29]. Besides, the (2 2 0) peaks for phosphorus-containing PtRuP/TFC samples shifted to even higher angles with increasing P content, which can be attributed to enhanced alloying of the bimetallic nanoparticles. The role of P, clearly seen to broaden the diffraction peaks, is to decrease the particle sizes with increasing addition of P. The sizes of the PtRuP nanoparticles, as determined by Scherrer's equation from the (2 2 0) peaks, are 3.9, 3.4, 2.9, and 2.2 nm for the mesoporous carbon-supported PtRu, $PtRuP_{0.05}$, $PtRuP_{0.1}$, and $PtRuP_{0.2}$ samples respectively. The particle sizes are reduced dramatically with increasing phosphorus contents.

The nitrogen adsorption–desorption isotherms of PtRuP/TFCs display a type IV isotherm curve with a H2-type hysteresis loop, as similar to those of TFC carbon and PtRu/TFC without P [9]. The textural properties as BET surface area, BJH pore size, and pore volume of the supported catalysts determined from the adsorption branch of corresponding isotherms are listed in Table 1. The surface areas and pore volumes of the PtRu/TFC with P addition, though all lower than that of PtRu/TFC without P, were nearly the same as in the level of ~770 m^2/g and ~0.66 cm^3/g, respectively. It is shown that high surface area and mesoporous structure of the carbon support can be retained after depositing 20 wt.% PtRuP nanoparticles. The dispersions of PtRuP nanoparticles with diverse amounts of P were similar.

In Fig. 2(a) TEM image of the mesoporous carbon TFC is displayed. The thin film morphology composed of well-ordered hexagonal carbon-rod arrays with pore size of 4.0 nm can be seen evidently. The thickness of perpendicular channel structure of the TFC as directly estimated from SEM image (Fig. 2(f)) is 70 nm on average. We should note that most of the platelets are stacked flat on the surface. The PtRu(P) nanocatalysts were thus homogeneously dispersed in the pore structure of TFC, as shown in Fig. 2(b)–(e). From the TEM images in Fig. 2 and our previously published cross-sectioned image [9], we know most of the metal particles are inside the nanochannels. The average particle size as directly determined from TEM images of the $PtRuP_{0.1}$/TFC sample is 3.6 nm, which is smaller than the one without P (4.3 nm). It is shown that the size of PtRu alloy nanoparticle can be effectively reduced by the incorporation of trace amount of non-metal phosphorus. The mesoporous carbon we made was replicated from SBA-15 silica and gave a structure mainly composed of solid carbon rods (see Fig. 2(a)) and side-supports (from the micropores of SBA-15) between the rods. The mesopore of the TFC material is the space in between the solid carbon rods. The pore structure is not of cylinder shape as the pores of SBA-15. The BJH pore size, as determined from nitrogen adsorption assuming a cylindrical pore shape, is only a rough estimation. Moreover, the BJH method is known to under-estimate the pore size. The particle size would not lead to much blockage of the channels. The pores between the carbon rods are very much open (interconnected).

3.2. Electrochemical property

The electrochemical activities of carbon-supported PtRuP catalyst as an anodic material in DMFC were examined by cyclic voltammetry (CV). All of the CV curves show voltammetric characteristics as typical electrooxidation of methanol on Pt-based bimetallics [30] (Fig. 3). All of the samples with P incorporation give enhanced anodic peak currents compared to that of the PtRu/TFC without phosphorus. In addition, the PtRuP/TFCs give superior current densities than a commercial Johnson-Matthey (*JM*) catalyst similar PtRu content (20 wt.% PtRu/XC-72 with a Pt:Ru = 1:1 atomic ratio and an average particle size of 2.2 nm). Various data derived from the CV results for the electrochemical oxidation of methanol are summarized in Table 2. The supported nanocatalyst with Pt:Ru:P = 1:1:0.1 gives a mass current density of 385.0 mA/mg_{PtRu} at 0.5 V which are the highest current density and the lowest onset potential. This shows that phosphorus promotes very well the catalytic efficiency for methanol oxidation and for Pt–Ru alloy. The PtRuP/TFCs reveal lower I_f/I_b values than that of the PtRu/TFC with no P incorporation. It may be because of metal nanocatalyst with smaller particle size to give more the accumulation of intermediate carbonaceous species on the metal surface in the reaction, thus showing a little weaker CO tolerance [30] (Fig. 3 and Table 2).

The long-term stability of supported PtRuP nanocatalysts evaluated by repeated CV scans is shown in Fig. 4. The $PtRuP_{0.2}$/TFC gives the highest activity in few initial scans but decreased gradually. For the smallest nanoparticle of $PtRuP_{0.2}$ (2.2 nm) provides high initial active surface area in reacting with methanol but suffers more CO poisoning effect in the meantime. The activity decay may be also due to unfavorable dispersion of the bimetal and gradual deformation of alloy nanoparticles during the reaction [31]. It is said that the bimetallic PtRu may (a) lose of active surface by the CO poisoning or particle aggregation, and (b) lose of Ru by the Ru dissolution. These problems can be more serious in small size nanoparticles such as $PtRuP_{0.2}$/TFC. On the other hand, $PtRuP_{0.1}$/TFC gives fairly stable high reactivity in the repeated CV runs. The mesocarbon-supported $PtRuP_{0.1}$ nanocatalyst with particle size of 2.9 nm gives superior catalytic performance and at the same time good stability in the acidic cell environment.

3.3. Composition and structure of the supported PtRuP nanocatalyst

The structures of supported PtRuP ternary nanocatalysts were characterized by XPS, ICP-AES, and EXAFS analyses to understand the chemical state, composition, and alloying degree. The XPS results are summarized in Table 3, with Pt $4f_{7/2}$ region deconvo-

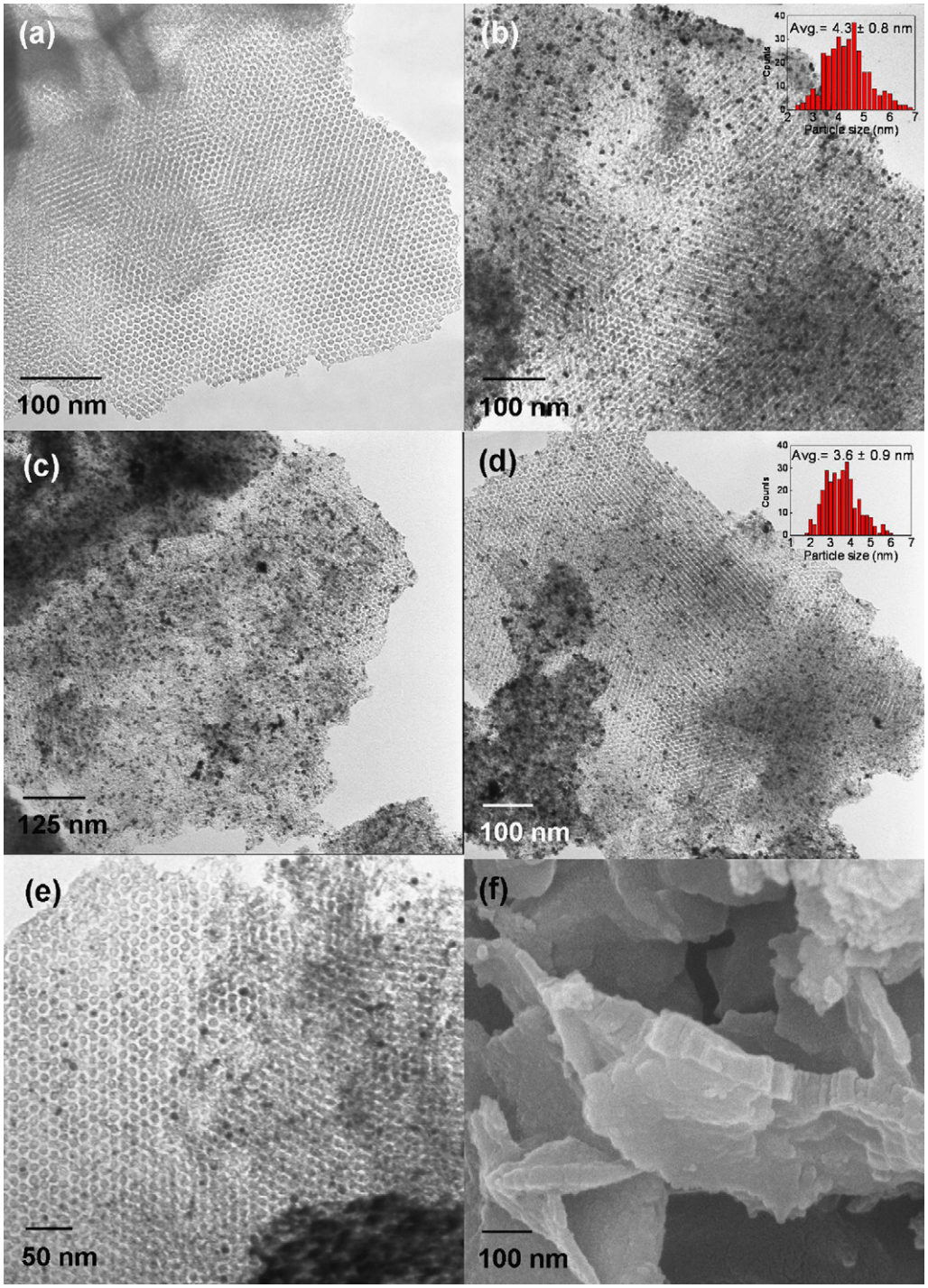

Fig. 2. The TEM images of (a) TFC carbon, (b) PtRu/TFC, (c) $PtRuP_{0.05}$/TFC, (d) $PtRuP_{0.1}$/TFC, (e) $PtRuP_{0.2}$/TFC, and (f) SEM image of TFC carbon.

Table 2
Methanol electrochemical oxidation activities over selected samples.

Sample[a]	Onset potential (V)	I_f/I_b value	Current density (mA/mg_{PtRu}) at 0.5 V	PtRu(P) particle size[b] (nm)
PtRu/TFC	0.350	3.01	242.5	3.9
$PtRuP_{0.05}$/TFC	0.344	2.38	348.8	3.4
$PtRuP_{0.1}$/TFC	0.328	2.29	385.0	2.9
$PtRuP_{0.2}$/TFC	0.337	1.66	362.5	2.2
JM PtRu/C	0.356	1.33	178.8	2.2

[a] All the samples are 20 wt.% PtRu(P) loading amounts.
[b] The PtRu(P) nanoparticle sizes are calculated by Scherrer's equation from the (2 2 0) diffraction peak of XRD results.

Table 3
XPS analyses for selected samples.

Sample	C 1s	Pt $4f_{7/2}$	Ru $3d_{5/2}$	Ru $3p_{3/2}$	Pt/Ru XPS	Pt/P XPS
$PtRuP_{0.2}$/TFC	284.5 (78) 285.7 (19) 287.3 (03)	71.3 (67) 72.6 (22) 73.9 (11)	280.9	461.9 (38) 463.2 (39) 465.0 (23)	1.64	1.51
$PtRuP_{0.1}$/TFC	284.5 (77) 285.4 (18) 286.8 (05)	71.6 (62) 72.7 (25) 73.9 (13)	281.3	461.6 (40) 463.2 (36) 465.9 (24)	1.61	6.68
$PtRuP_{0.05}$/TFC	284.4 (77) 285.4 (16) 286.8 (07)	71.2 (64) 72.4 (22) 73.6 (14)	281.2	462.1 (26) 463.5 (56) 466.3 (18)	1.65	—[a]
PtRu/TFC	284.5 (75) 285.5 (21) 287.3 (04)	71.3 (71) 72.5 (21) 73.8 (08)	281.4	462.1 (39) 463.6 (39) 465.5 (22)	1.71	—

[a] P 2p is at noise level.

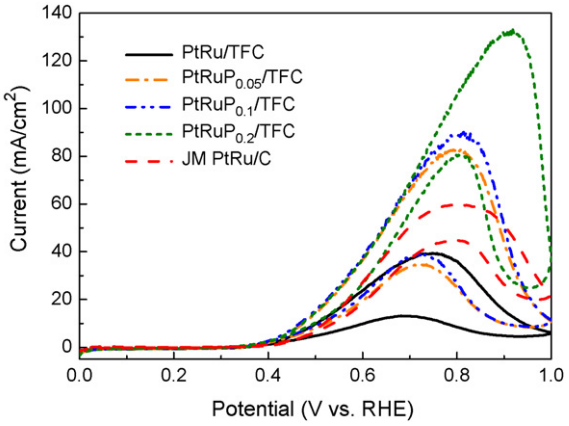

Fig. 3. Cyclic voltammogram curves over selected samples. The curves are collected in 0.5 M H_2SO_4 and 1.0 M CH_3OH solution with scan rate 10 mV/s at 60 °C.

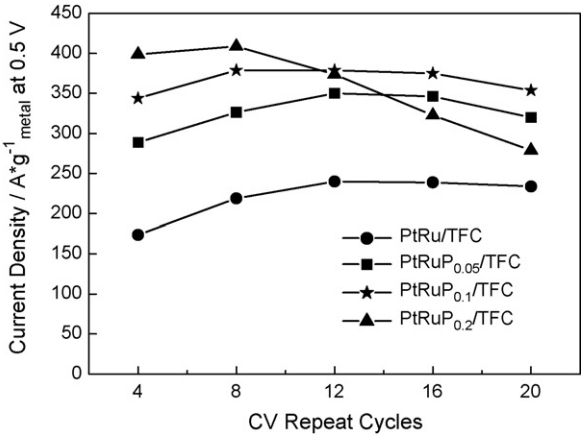

Fig. 4. Stability tests with regard to repeated CV cycles for selected samples. The specific current densities are deduced from the corresponding anodic currents at 0.5 V.

luted into corresponding Pt metal, PtO or $Pt(OH)_2$, and PtO_2 species, and Ru $3p_{3/2}$ region into Ru metal, anhydrous RuO_2, and hydrous amorphous RuO_xH_y species. All of the PtRu(P)/TFC samples exhibit Pt metal and Ru oxide as the dominant states and a Pt-rich surface segregation of the alloy nanoparticles. The result is similar to our previous work on PtRu catalysts on mesoporous carbon with ozone treatment and wet-chemical reduction approach [32]. There is little alteration in the ratios of Pt/Ru of surface PtRu structure upon loading of P showing no obvious change with increased P contents. The XPS spectra for the P 2p peaks for all of the PtRuP/TFC samples (figure not shown) give rather weak and noisy signals due to the small phosphorus content, however, a main peak at ~133.0 eV could be identified and implied that most of P existed in oxidized form. No recognizable element state (130 eV) or metal phosphide (129 eV) could be identified [22]. For the small Pt/P values of 1.51 for $PtRuP_{0.2}$/TFC and 6.68 for $PtRuP_{0.1}$/TFC, phosphorus is thus most on the exterior surface of PtRu alloy particle. It is then considered that P coexists with PtRu nanoparticle as capping agent and most of P is in oxidized state without forming interstitial compounds. The quantitative elemental analyses are estimated by ICP-AES in Table 4, which show that in all of PtRu(P)/TFC samples the Pt/Ru composition are about the same. The higher Pt/P values as compared to those measured by XPS confirm again that P mostly resides on the surface of PtRu nanoparticles. Also the ratios of Pt/Ru are higher as measured by XPS compared to ICP-AES values indicate the element Pt is enriched on the surface of the PtRu nanoparticles.

The radial distribution functions at Pt L_{III}-edge by Fourier transformation of k^3-weighted EXAFS data for those PtRu(P)/TFCs are shown in Fig. 5. All of the samples with phosphorus addition give similar patterns to that of PtRu/TFC without phosphorus incorporation, which indicate that no change in the alloy structure of PtRu upon loading of P [33]. Comparing to the *JM* PtRu/C catalyst with a 2.2 nm-sized metal particle and high alloying extent, the 20 wt.% PtRuP/TFCs exhibited somewhat lower degrees of alloying in the PtRu bimetallic nanocatalysts. In Table 5, structure parameters derived from curve-fitted EXAFS data at Pt L_{III}-edge and Ru K-edge

Table 4
ICP-AES elemental analyses for selected samples.

Sample	Pt (wt.%)	Ru (wt.%)	P (wt.%)	Pt/Ru[a]	Pt/P[b]
$PtRuP_{0.2}$/TFC	14.0	5.18	0.555	1.40	4.01
$PtRuP_{0.1}$/TFC	14.6	5.52	0.176	1.37	13.18
$PtRuP_{0.05}$/TFC	14.5	5.35	—[c]	1.40	—
PtRu/TFC	16.3	4.77	—	1.77	—

[a] Pt/Ru = (Pt (wt.%)/195.1)/(Ru (wt.%)/101.1).
[b] Pt/P = (Pt (wt.%)/195.1)/(P (wt.%)/31.0).
[c] At noise level.

Table 5
Curve-fitting results of the EXAFS data at Pt L_{III}-edge[a] and Ru K-edge[b] over selected samples.

Sample	Shell	N[c]	R (Å)	σ^2 (Å^2)	r-Factor
Pt L_{III}-edge					
$PtRuP_{0.2}$/TFC	Pt–Pt	8.2 ± 0.9	2.747 ± 0.028	0.007	0.0050
	Pt–Ru	1.5 ± 0.7	2.684 ± 0.090	0.005	
$PtRuP_{0.1}$/TFC	Pt–Pt	8.4 ± 1.1	2.745 ± 0.030	0.007	0.0054
	Pt–Ru	1.2 ± 0.7	2.685 ± 0.090	0.004	
$PtRuP_{0.05}$/TFC	Pt–Pt	8.7 ± 0.8	2.749 ± 0.026	0.007	0.0033
	Pt–Ru	1.3 ± 0.6	2.688 ± 0.086	0.005	
PtRu/TFC	Pt–Pt	8.8 ± 0.5	2.754 ± 0.021	0.009	0.0017
	Pt–Ru	1.2 ± 0.4	2.713 ± 0.064	0.004	
Ru K-edge					
$PtRuP_{0.2}$/TFC	Ru–Ru	3.9 ± 0.5	2.652 ± 0.014	0.007	0.0014
	Ru–Pt	2.4 ± 0.5	2.697 ± 0.031	0.005	
$PtRuP_{0.1}$/TFC	Ru–Ru	3.9 ± 0.8	2.651 ± 0.015	0.008	0.0044
	Ru–Pt	2.8 ± 1.0	2.695 ± 0.029	0.007	
$PtRuP_{0.05}$/TFC	Ru–Ru	4.3 ± 0.7	2.658 ± 0.008	0.008	0.0024
	Ru–Pt	2.0 ± 0.7	2.698 ± 0.032	0.004	
PtRu/TFC	Ru–Ru	4.3 ± 0.7	2.658 ± 0.008	0.008	0.0035
	Ru–Pt	2.2 ± 0.7	2.670 ± 0.032	0.008	

[a] Pt L_{III}-edge $k^3\chi(k)$ data in the k-space from 3.0 to 14.3 Å^{-1} is Fourier transformed to r-space. Numerical fittings are carried out with regard to the data in r-space ranging from 1.60 to 3.10 Å.
[b] Ru K-edge is conducted with the k-space from 3.5 to 12.9 Å^{-1}, and the r-space from 1.69 to 3.10 Å.
[c] N: coordination number, R: coordination distance, σ^2: Debye–Waller factor.

are summarized. One can notice that the coordination numbers of Pt–Pt and Ru–Ru homometallic bondings are reduced gradually with the increasing of P. In other words, the size of PtRu bimetallic cluster is reduced to some extent by the element P. The result is in good agreement with size estimation from XRD which gives reduced particle sizes of PtRu bimetallics upon loading of P evidently.

3.4. Enhanced catalytic reactivity and stability by phosphorus incorporation

We have reported in this work the PtRu nanocatalysts supported on mesoporous carbon thin film with the loading of element P for electrochemical oxidation of methanol. The mesoporous carbon TFC having unique thin film morphology (Fig. 2) in assisting catalytic performance by providing abundant active metal sites and facilitating the transport of reactants and products both through the mesopores. For and much enhanced current densities in the PtRuP/TFCs (compared to PtRu/TFC), the element P helps to decrease the particle sizes to give more active sites but phosphorus does not change appreciably the electronic structure of PtRu. The synergy between Pt and Ru surface atom ensemble, consisting of Pt-rich sites for methanol adsorption and subsequent transformation and adjacent Ru sites for assisting the completed electrooxidation of methanol, is well-preserved [34,35]. The incorporation of phosphorus in the growth of PtRu bimetallics helps the reduction of size of nanoparticle by reducing surface energy. From the XPS results in Table 3, the distribution of P is near the surface of the PtRu particle and in mostly oxidized form. The phosphorus functions as a surfactant in lowering surface energy of the metal nanoparticle to limit its size while gives very little electronic perturbation. The r-space EXAFS data at Pt reveal little change in the structure upon loading of P. The contribution of Pt–P or Ru–P coordination is too little to be determined in the curve-fitting analysis. Nevertheless, some metal surface-binding of P is expected in the PtRuP nanoparticle, which is considered as the main factor in reducing the size of PtRu. Moreover, for a very small Pt-based nanoparticle, the dissolution of second metal is a major problem for long-term stability. The $PtRuP_{0.1}$/TFC with particle size of 2.9 nm not only shows much enhanced current density in the electrochemical reaction but also gives good stability comparable to PtRu/TFC. The surface-incorporated trace amount of P may stabilize the small nanoparticle considerably from aggregation and deformation in the acidic reaction medium at 60 °C.

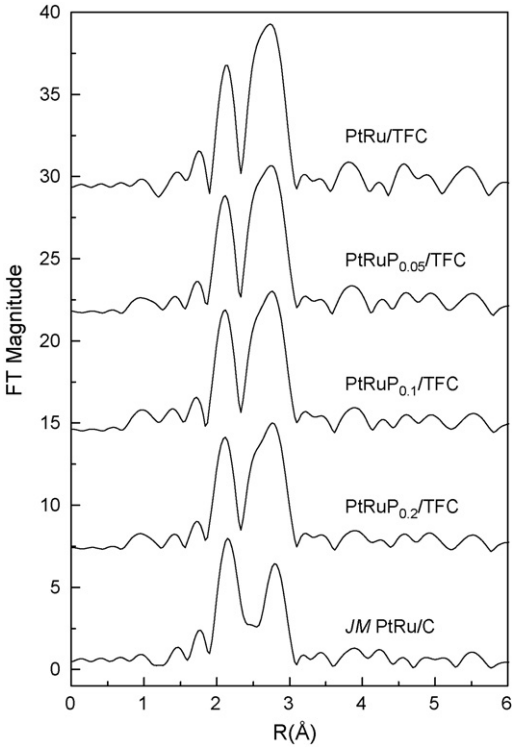

Fig. 5. Fourier-transformed k^3-weighted EXAFS data at Pt L_{III}-edge for selected samples.

4. Conclusion

With the incorporation of the non-metallic element phosphorus, the PtRuP nanocatalysts, highly dispersed on mesoporous carbon thin film with perpendicular channels, are found to give excellent activity in the electrochemical oxidation of methanol. The morphology of perpendicular channels of the carbon TFC not only benefits the dispersion of metal nanocatalyst but also facilitates the transport of fuel and product in its mesopore. The 20 wt.% $PtRuP_{0.1}$/TFC gives the highest catalytic current density of 385 mA/mg_{PtRu}, which is 2.1 times superior to that of a commercial *JM* PtRu/C catalyst and 1.6 times higher than the PtRu/TFC without phosphorus. Trace amount of the additive P acts both to increase the active metal sites by decreasing the size of PtRu nanoparticle and to enhance the catalytic stability by keeping the bimetallics from aggregation and dissolution. The XPS characterization shows that the phosphorus exists in an oxidized form located in the exterior surface of PtRu alloy, and the EXAFS data give little change of the electronic state of Pt with P incorporation. The phosphorus is responsible for the protection of small PtRu particle form deformation in the reaction, therefore the synergy in bifunctional effect can be well-preserved for long-term catalytic stability. We consider both effects, good transport and catalytically active PtRu small particles, are important for a well-performed electrode catalyst. The ordered mesoporous carbon-supported PtRuP nanocatalyst is found to give excellent catalytic reactivity and stability in the electrooxidation of methanol.

Acknowledgements

The research was supported by a grant from the National Science Council, Taiwan. We are grateful to NSRRC for generous X-ray beamtime for EXAFS measurements.

References

[1] K.Y. Chan, J. Ding, J.W. Ren, S.A. Cheng, K.Y. Tsang, J. Mater. Chem. 14 (2004) 505.
[2] H.S. Liu, C.J. Song, L. Zhang, J.J. Zhang, H.J. Wang, D.P. Wilkinson, J. Power Sources 155 (2006) 95.
[3] O.A. Petrii, J. Solid State Electrochem. 12 (2008) 609.
[4] A. Stein, Z.Y. Wang, M.A. Fierke, Adv. Mater. 21 (2009) 265.
[5] G.S. Chai, S.B. Yoon, J.S. Yu, J.H. Choi, Y.E. Sung, J. Phys. Chem. B 108 (2004) 7074.
[6] J. Ding, K.Y. Chan, J.W. Ren, F.S. Xiao, Electrochim. Acta 50 (2005) 3131.
[7] S.-H. Liu, W.-Y. Yu, C.-H. Chen, A.-Y. Lo, B.-J. Hwang, S.-H. Chien, S.-B. Liu, Chem. Mater. 20 (2008) 1622.
[8] J.R.C. Salgado, J.J. Quintana, L. Calvillo, M.J. Lazaro, P.L. Cabot, I. Esparbe, E. Pastor, Phys. Chem. Chem. Phys. 10 (2008) 6796.
[9] M.-L. Lin, C.-C. Huang, M.-Y. Lo, C.-Y. Mou, J. Phys. Chem. C 112 (2008) 867.
[10] W. Chen, J. Kim, L.-P. Xu, S. Sun, S. Chen, J. Phys. Chem. C 111 (2007) 13452.
[11] Z.X. Liang, T.S. Zhao, J.B. Xu, J. Power Sources 185 (2008) 166.
[12] Z.-B. Wang, P.-J. Zuo, G.-J. Wang, C.-Y. Du, G.-P. Yin, J. Phys. Chem. C 112 (2008) 6582.
[13] K.-W. Park, J.-H Choi, S.-A. Lee, C.H. Pak, H. Chang, Y.-E. Sung, J. Catal. 224 (2004) 236.
[14] Y.M. Liang, H.M. Zhang, H.X. Zhong, X.B. Zhu, Z.Q. Tian, D.Y. Xu, B.L. Yi, J. Catal. 238 (2006) 468.
[15] P. Strasser, J. Comb. Chem. 10 (2008) 216.
[16] S. Siracusano, A. Stassi, V. Baglio, A.S. Arico, F. Capitanio, A.C. Tavares, Electrochim. Acta 54 (2009) 4844.
[17] Y. Takasu, H. Itaya, T. Iwazaki, R. Miyoshi, T. Ohnuma, W. Sugimoto, Y. Murakami, Chem. Commun. (2001) 341.
[18] X.X. Li, X.P. Qiu, H.P. Yuan, L.Q. Chen, W.T. Zhu, J. Power Sources 184 (2008) 353.
[19] S.H. Joo, K. Kwon, D.J. You, C. Pak, H. Chang, J.M. Kim, Electrochim. Acta 54 (2009) 5746.
[20] C. Bock, C. Paquet, M. Couillard, G.A. Botton, B.R. MacDougall, J. Am. Chem. Soc. 126 (2004) 8028.
[21] W.Z. Li, C.H. Liang, W.J. Zhou, J.S. Qiu, H.Q. Li, G.Q. Sun, Q. Xin, Carbon 42 (2004) 436.
[22] H. Daimon, Y. Kurobe, Catal. Today 111 (2006) 182.
[23] X.Z. Xue, J.J. Ge, C.P. Liu, W. Xing, T.H. Lu, Electrochem. Commun. 8 (2006) 1280.
[24] X.Z. Xue, J.J. Ge, T. Tian, C.P. Liu, W. Xing, T.H. Lu, J. Power Sources 172 (2007) 560.
[25] S. Suzuki, Y. Ohbu, T. Mizukami, Y. Takamori, M. Morishima, H. Daimon, M. Hiratani, J. Electrochem. Soc. 156 (2009) B27.
[26] Y. Takasu, T. Kawaguchi, W. Sugimoto, Y. Murakami, Electrochim. Acta 48 (2003) 3861.
[27] E.A. Stern, M. Newville, B. Ravel, Y. Yacoby, D. Haskel, Physica B 209 (1995) 117.
[28] D. Chu, S. Gilman, J. Electrochem. Soc. 143 (1996) 1685.
[29] A.S. Arico, P. Creti, H. Kim, R. Mantegna, N. Giordano, V. Antonucci, J. Electrochem. Soc. 143 (1996) 3950.
[30] Z.L. Liu, X.Y. Ling, X.D. Su, J.Y. Lee, J. Phys. Chem. B 108 (2004) 8234.
[31] H.A. Gasteiger, N.J. Markovic, P.N. Ross, E.J. Cairns, J. Phys. Chem. 97 (1993) 12020.
[32] M.-L. Lin, M.-Y. Lo, C.-Y. Mou, J. Phys. Chem. C 113 (2009) 16158.
[33] S. Alayoglu, P. Zavalij, B. Eichhorn, Q. Wang, A.I. Frenkel, P. Chupas, ACS Nano 3 (2009) 3127.
[34] A. Cuesta, J. Am. Chem. Soc. 128 (2006) 13332.
[35] C. Roth, N. Benker, R. Theissmann, R.J. Nichols, D.J. Schiffrin, Langmuir 24 (2008) 2191.